

1 **Study of Different Solar Cycle Variations of Solar**
2 **Energetic Particles and Cosmic Rays by Despiking**
3 **ACE/SIS Heavy-Ion Fluxes**

G. Qin, and L.-L. Zhao

4 State Key Laboratory of Space Weather, Center for Space Science and
5 Applied Research, Chinese Academy of Sciences, P.O. Box 8701, Beijing
6 100190, China

G. Qin, State Key Laboratory of Space Weather, Center for Space Science and Applied Research, Chinese Academy of Sciences, P.O. Box 8701, Beijing 100190, China, (gqin@spaceweather.ac.cn)

L.-L. Zhao, State Key Laboratory of Space Weather, Center for Space Science and Applied Research, Chinese Academy of Sciences, P.O. Box 8701, Beijing 100190, China, (llzhao@spaceweather.ac.cn)

7 **Abstract.** Cosmic Rays (CRs) include Galactic Cosmic Rays (GCRs) and
8 Anomalous Cosmic Rays (ACRs). The CR flux data of protons and heavy-
9 ions observed with spacecraft are often seriously contaminated by Solar En-
10 ergetic Particle (SEP) events. In this work, we separate SEPs from CRs of
11 ACE/SIS spacecraft observations with an automatic despiking algorithm, so
12 we are able to study the different variations of SEPs and CRs over a solar
13 cycle. In particular, we study the elemental ratio, first ionization potential
14 dependence and elemental dependence, and information entropy of SEPs and
15 CRs. So that we can gain new insights into energetic particles' different com-
16 positions, origins, and transport processes, etc.

1. Introduction

17 The Solar Energetic Particles (SEPs) are high energy particles produced by solar events
18 with abrupt variations with the process of solar events. In addition, the Cosmic Rays
19 (CRs), including Galactic Cosmic Rays (GCRs) and Anomalous Cosmic Rays (ACRs),
20 of protons and heavy-ions can be assumed as a background gradually evaluating over the
21 solar cycle. Therefore, CRs and SEPs have distinctively different behaviours varying with
22 solar activities. Furthermore, ACRs and GCRs are also obviously different, since ACRs
23 are usually believed to be accelerated by termination shock of heliosphere, while GCRs
24 have sources outside the heliosphere.

25 However, GCRs from spacecraft observations are often significantly contaminated by
26 SEP events, especially during solar maximum. Recently, *Qin et al.* [2012] used a robust
27 despiking algorithm based on the Poincare map thresholding method [*Goring and Nikora,*
28 2002] to eliminate the spiked flux records possibly associated with SEP events from con-
29 tinuous GCR records. Based on this method, *Zhao and Qin* [2013] and *Zhao et al.* [2013]
30 used the despiking algorithm to remove the spikes of ACE/SIS flux to obtain the clean
31 background of CRs. Furthermore, using the GCR data from ACE/CRIS, *Zhao and Qin*
32 [2013] developed an observation-based elemental GCR heavy-ion spectra model. It is
33 shown that the model, if extrapolated, agrees with the GCR data from ACE/SIS with
34 despiking very well.

35 *Reames* [2013] studied the abundances of the heavy elements in SEPs with energy 2–15
36 MeV/nuc measured on Wind spacecraft during 54 large SEP events for the period over
37 17 years. It is shown that the coronal abundances can be determined from SEP mea-

surements, and their value relative to those in the solar photosphere depend on the first ionization potential (FIP) of the element. Furthermore, Shannon entropy (also named as information entropy) is a commonly used quantity to characterize the degree of uncertainty and/or the information contained in a time-series signal. *Laurenza et al.* [2012] used information entropy as a proxy of changes of spectrum shape in a limited energy range to study the evolution of the differential flux spectrum during an SEP event. By investigating the time profile of Shannon entropy during an SEP event, they concluded that a perpendicular shock in the solar corona produced the particle acceleration of the event.

In the study of SEPs, usually fluxes in different phases of individual SEP events are studied carefully. However, in this work, we demonstrate that it is feasible to study the different characteristics of SEPs and CRs (GCRs or ACRs), by separating their records in spacecraft observations over solar cycles automatically with the aforementioned despiking algorithm. The article is organized as follows. We discuss the despiking of ACE/SIS heavy ions to separate CRs from SEPs in section 2. The elemental fluxes and their ratios for SEPs and CRs are discussed in section 3. The first ionization potential dependence of SEP fluxes and elemental dependence of CR fluxes are discussed in subsections 4.1 and 4.2, respectively. The shannon entropy of CRs and SEPs from heavy ions are shown in section 5. Finally, discussion and conclusion are presented in section 6.

2. Data and Despiking Algorithm

The NASA Advanced Composition Explorer (ACE) spacecraft has greatly extended our ability to explore the heavy nuclei over a wide energy range [*Stone et al.*, 1998], and the flux measurements from ACE spacecraft are the most reliable and statistically significant

60 heavy-ion data so far, due to their large geometrical acceptance and excellent charge and
 61 mass resolution [*George et al.*, 2009].

62 In this study, we use heavy-ion flux data from the Solar Isotope Spectrometer (SIS)
 63 instrument onboard ACE spacecraft. The SIS instrument is designed to provide high
 64 resolution measurements of the isotopic composition of energetic nuclei from He to Ni
 65 over the energy range 10 MeV/nuc - 100 MeV/nuc. It records SEPs during large solar
 66 events, and CRs (GCRs or ACRs) during solar quiet time, so we are provided a unique
 67 opportunity to compare the different characteristics between SEPs and CRs (GCRs or
 68 ACRs).

69 The flux measurements for heavy elemental species (atomic number $2 \leq z \leq 28$) of the
 70 SIS (if available) at level 2 over the period from the year 1997 to 2013 are readily obtained
 71 from the ACE Science Center, with recommended energy (E_i) in unit of MeV/nuc of each
 72 energy interval shown in Table 1. Then, we use He(2) data of SIS measurements to flag
 73 periods of spikes, possibly associated with SEP events, with a despiking algorithm [*Qin*
 74 *et al.*, 2012] [see also, *Zhao and Qin*, 2013] based on the Poincare Map Thresholding
 75 method [*Goring and Nikora*, 2002]. Specifically, we go through the last five SIS He
 76 channels (> 8 MeV/nuc), at any time if one of the He channels is considered as a spike
 77 with the despiking algorithm, the period is flagged as solar activity. Here, the Universal
 78 threshold $\lambda_U = 1.1$ in the thresholding algorithm [*Qin et al.*, 2012]. Note that the data
 79 from SIS instrument include a “solar activity flag” too (noted as “SIS flag” hereafter)
 80 that flags periods with significant SEP contributions. Figure 1 illustrates the percentage
 81 of flagged one-day-periods in each year from year 1998 to year 2013 with SIS flag (top
 82 panel) and our flag (bottom panel). The two panels of Figure 1 generally show similar

83 variation patterns. In addition, we investigate the flagged one-hour-periods and get an
 84 “event” for each consecutive range of flagged periods. Here, we assume an event as an
 85 impulsive one if it lasts less than a day, otherwise, it is assumed as a gradual one. We
 86 find that of all the events only a few are impulsive ones, so this method is only good at
 87 distinguish gradual solar events from CRs background. In the next, we get our flag using
 88 the despiking algorithm [*Qin et al.*, 2012] with a computer automatically and discard the
 89 impulsive events and divide the rest data into two groups, the gradual SEP data during
 90 the flagged periods and the CR data during the non-flagged periods.

91 Figure 2 shows the kinetic energy spectra of element O for the year 1998 (left panel,
 92 solar minimum) and the year 2001 (right panel, solar maximum). The blue lines indicate
 93 raw data from SIS measurements, the red lines indicate SEP data from flagged periods,
 94 and the black lines indicate CR background data from the non-flagged periods. From the
 95 figure we can see, that during the solar minimum the CR data are much higher than that
 96 during the solar maximum, but the SEP data are much lower than that during the solar
 97 maximum. In addition, for the CR data, the energy range with positive spectral index
 98 indicates GCR, while that with negative spectral index indicates ACR, so it is shown that
 99 the upper limit of ACR dominate energy range is much larger during the solar minimum.

3. Flux Ratio for SEP and CR Data

100 The SIS instrument measures the differential flux of each element over 8 different con-
 101 secutive energy intervals. In order to study flux ratio for SEP and CR data, we choose
 102 three energy channels, I, II, and III with energy approximately equal to 13, 31, and 46
 103 MeV/nuc, respectively, for each of N, O, and Fe as shown in Table 2. In Table 2, E_i
 104 shows the energy channel for each of N, O, and Fe shown in Table 1. Note that the

105 measurements of 13 MeV/nuc channels of N and O are considered mainly from ACRs,
106 that the flux of 31 MeV/nuc channels of N and O are considered dominated with GCRs
107 with some contribution from ACRs, and that of the rest channels are mainly from GCRs
108 with much less ACRs contribution.

109 Figure 3 shows despiked monthly fluxes, or CRs, of O (blue circles), Fe (purple triangles),
110 and N (cyan triangles) with energy channels 13 MeV/nuc (top pannel), 31 MeV/nuc
111 (middle pannel), and 46 MeV/nuc (bottom panel). Note that the grey line indicates
112 the time variations of sunspot numbers (SSN). It is shown that for all the O, N, and Fe
113 channels the CR fluxes are anti-correlated with SSN. In addition, O and N channels show
114 stronger anti-correlation than Fe channels, especially for the lowest energy channel, 13
115 MeV/nuc.

116 Figure 4 is similar as Figure 3 except that the color symbols indicate SEP fluxes in
117 monthly and yearly average in left and right panels, respectively. It is shown that the
118 SEP fluxes have much larger variations in any epoch of solar activity, which is a typical
119 behavior for gradual SEPs [Reames, 2013]. In addition, the SEP fluxes also show moderate
120 correlation with solar cycles, and the correlation is stronger for lower energy channels. In
121 addition, the fluxes are larger during solar maximum and descending phases than that
122 during solar minimum and ascending phases.

123 Figure 5 is similar as Figure 4 except that red and blue symbols indicate Fe/O ratio and
124 N/O ratio, respectively, and that circles and triangles indicate SEPs and CRs, respectively.
125 From the figure we can see the Fe/O ratio of CRs in monthly average is obviously correlated
126 to the solar activity in lower two energy channels, but the correlation in the highest energy
127 channel is much smaller, indicating different modulation process of ACRs and GCRs under

128 varied modulation strength. In addition, it is found that the Fe/O ratio of SEPs have
 129 very large variations in any solar cycle epoch. Although the distribution of Fe/O ratio
 130 of SEPs are scattering, the ratio is distinctly higher than that of CR. However, the N/O
 131 ratio of SEPs shows much less variations in any solar cycle epoch, and both of CRs and
 132 SEPs of N/O don't show much solar activity correlation. In addition, the yearly average
 133 of N/O ratio of CRs is usually larger than that of SEPs. Furthermore, the ratio N/O of
 134 CRs and SEPs are generally larger than the ratio Fe/O of CRs and SEPs, respectively.

135 For the ratio of Fe/O of 13 MeV/nuc CR particles, the apparent solar cycle variations
 136 are caused by the strong solar cycle dependence of ACR flux of O and weak solar cycle
 137 dependence of GCR flux of Fe. And for the ratio of Fe/O of 31 MeV/nuc CR particles,
 138 there is similar but much weaker solar cycle dependence because in 31 MeV/nuc O channel,
 139 ACRs are not dominated as that in 13 MeV/nuc O channel, and the solar cycle dependence
 140 of 31 MeV/nuc O CRs is relatively weaker and the solar cycle dependence of 31 MeV/nuc
 141 Fe CRs is relatively stronger than that with energy 13 MeV/nuc.

4. First Ionization Potential Dependence of SEP Fluxes and Elemental Dependence of GCR Fluxes

142 In order to obtain the flux at any energy per nucleon, E , for any heavy nuclei n , we
 143 get the energy channels E_i and E_{i+1} with $E_i \leq E \leq E_{i+1}$ in Table 1. For each year t
 144 from 1998 to 2013 we fit the yearly averaged SEP and CR fluxes of each heavy ACE/SIS
 145 nuclei n from channel E_i to E_{i+1} shown in Table 1 with $f_{SEP}^F(n, E, t) = f_{SEP0}(n, t)E^{k(n,t)}$
 146 and $f_{CR}^F(n, E, t) = f_{CR0}(n, t)E^{q(n,t)}$, respectively. From the fitting result, we can get the
 147 SEP at $E = 15$ MeV/nuc and GCR at $E = 30$ MeV/nuc, for each year and element,
 148 $f_{SEP}^F(n, 15 \text{ MeV/nuc}, t)$ and $f_{CR}^F(n, 30 \text{ MeV/nuc}, t)$, respectively. Note that from Figure

1 we can see in the years 1999 and 2006 to 2010, the percentage of flagged periods with
 2 our flag is all smaller than 30%, so below we do not get fitting of SEPs in these years
 3 because of too few SEP events. In next two subsections, we study different dependence
 4 of SEP fluxes of 15 MeV/nuc and GCR fluxes of 30 MeV/nuc.

4.1. First Ionization Potential Dependence of SEP Fluxes Relative to Photospheric Abundances

5 *Reames* [2013] showed that SEP abundances divided by recent photospheric abundances
 6 can be approximately represented as a power law of First Ionization potential (FIP).

7 Figure 6 illustrates the fitted yearly SEP fluxes at 15 MeV/nuc divided by recent pho-
 8 tospheric abundances as a function of FIP from the year 1998 to 2013, except the years
 9 1999, and 2006-2010, in arbitrary unit. Note that the results are multiplied by a free
 10 parameter for the purpose of presentation and that the recent photospheric abundances
 11 of elements and FIP are taken from Table 1 of *Reames* [2013]. It is shown that the 15
 12 MeV/nuc SEP fluxes divided by photospheric abundances are linearly correlated with FIP
 13 in log-log space, with fitted slopes, intercepts, and correlation coefficients.

14 In Figure 7 we show the fitted slopes, correlation coefficients (Corr. Coef.), and inter-
 15 cepts of the above linear relationship. Top left panel of the figure shows the slopes, Corr.
 16 Coef., and sunspot numbers (SSN) varying as the year. It is shown that the Corr. Coef.
 17 of the linear relationship in Figure 6 are all near -1 , indicating a strong anti-correlation.
 18 And the top right panel shows the slopes and Corr. Coef. varying as the SSN, we can see
 19 when SSN is large, the Corr. Coef. is near -1 , indicating stronger linear-relationship in
 20 Figure 6. Furthermore, the slopes and Corr. Coef. can be linearly fitted as function of
 21 SSN with fitting correlation coefficients $R = -0.80$ and $R = -0.76$, respectively. More-

170 over, the bottom left panel shows the intercepts and SSN varying as the year. In addition,
 171 the bottom right panel shows the intercepts as a function of the SSN, and the intercepts
 172 can also be linearly fitted as a function of SSN with fitting correlation coefficient $R = 0.58$.

4.2. GCR Abundance Relative to Atomic Numbers

173 Figure 8 shows the fitted 30 MeV/nuc GCR flux as a function of element numbers for
 174 each year from 1997 to 2013. Note that the results are multiplied by a free parameter
 175 for the purpose of presentation. From the figure we can see that the GCR fluxes can be
 176 linearly fitted in log-log space with slopes, intercepts, and correlation coefficients (Corr.
 177 Coef.). Note that in Figure 8 the filled stars indicate Fe which is not included in the
 178 power law fitting (solid line) to remove the iron peak.

179 Similar as in Figure 7, the fitted slopes, intercepts, and correlation coefficients in Figure
 180 8 is shown in Figure 9. We can see the Corr. Coef. of the fitting results of GCRs in
 181 Figure 8 is nearer to -1 than that of SEPs in Figure 6, indicating better linear fitting of
 182 GCRs. Note that in order to linear-fit the slopes and intercepts from the fitting results in
 183 Figure 8, the SSN is one year delayed because there is such a delay of solar modulation
 184 for GCRs in heliosphere.

5. Shannon Entropy of SEPs and CRs

185 Following *Laurenza et al.* [2012], we use Shannon entropy (information entropy) to
 186 investigate the spectrum evolution of SEPs and CRs. Firstly, the entropy S can be written
 187 as

$$S = -k \sum_{i=1}^N p_i \ln p_i E_i, \quad (1)$$

188 where E_i denotes the i th energy interval, f_i denotes the corresponding flux, $p_i =$
 189 $f_i / \sum_{i=1}^N f_i E_i$ denotes the corresponding probability density, and k is a constant which is
 190 generally assumed as $k = 1 / \log(N)$.

191 Next, we calculate the yearly averaged ACE/SIS flux of element Si with all energy
 192 channels (11.0 MeV/nuc - 103.6 MeV/nuc) and that of O with the first four energy
 193 channels (< 20 MeV/nuc), for raw data, CRs (background data), and SEPs (spike data).
 194 Top panel of Figure 10 shows entropy of the element Si, and bottom panel shows entropy
 195 of the element O. In the figure, blue, red, and black lines indicate the raw data, the SEPs
 196 (spike data), and the CRs (background data), respectively. Similar as above, we do not
 197 include the SEPs data in the years 1999, and 2006-2010. It is noted that in top panel
 198 of Figure 10 the CRs data of Si are GCRs, and that in the bottom panel the CRs data
 199 of O are mostly ACRs. From the figure we can see, the entropy of GCRs of Si is almost
 200 a constant but that of the ACRs of O has weak solar cycle variations. In addition, the
 201 entropy of Si and O SEPs are smaller than that of Si GCRs and O ACRs, respectively.
 202 Furthermore, the entropy of raw data usually closely track that of SEPs, but during the
 203 recent extreme solar minimum, the entropy of raw data is almost identical to that of CRs
 204 because the raw data are dominated with CRs.

6. Discussion and Conclusion

205 In this work, we use a despiking method to automatically separate CRs, including GCRs
 206 and ACRs, from SEPs over the period more than one solar cycle for ACE/SIS heavy ion
 207 measurements, so that we are able to study solar cycle variations of CRs and SEPs in the
 208 same energy ranges simultaneously with a computer code. Finally, we have the following
 209 findings.

210 It is shown that CRs usually show solar cycle variations with different levels of strength
211 according to different energy and elements. In addition, although SEPs show much larger
212 variations in any epoch of solar activity, they still show moderate correlation with solar
213 cycles. The possible reason is that during solar maximum and descending phases, there are
214 more large solar events and in solar events there are more enhancements of seed particles
215 because of more preceding solar events, so the average SEP fluxes are larger than that
216 during solar minimum and ascending phases. Therefore, different elemental ratios, Fe/O
217 or N/O, for SEPs or CRs in different energy range show different solar cycle variations.

218 In addition, it is shown that the SEP fluxes relative to the recent photospheric abun-
219 dances of elements can be linearly fit with FIP in log-log space to get fitting slopes,
220 correlation coefficients, and intercepts. It is also shown that both slopes and correlation
221 coefficients show strong anti-correlation with SSN and that intercepts show correlation
222 with SSN when there are enough SEP events for statistics. However, for the same el-
223 ements CRs behave much differently. In each year, CR fluxes can be fit linearly with
224 atomic numbers in log-log space. In addition, the fitting slopes and intercepts can also be
225 fitted linearly with SSN with one year delay.

226 Furthermore, we find that for the same element in the same energy range, the variations
227 of Shannon entropy of GCRs are much smaller than that of the ACRs entropy, and the
228 SEPs entropy is usually smaller than that of CRs. It is known that when the uncertainty
229 of a system is increased, the Shannon entropy is increased. And also since the SEPs are
230 associated with solar eruptions with evolution in days, but CRs have much longer time
231 of evolution, so CRs have much larger uncertainty than SEPs. Therefore, SEPs usually
232 have smaller value of Shannon entropy than CRs. In addition, the sources of ACRs are

233 inside heliosphere and modified by solar activity, but the sources of GCRs are outside
234 heliosphere, so the solar cycle variation of ACRs entropy is larger than GCRs entropy.

235 The above results from data analysis are useful for us to understand different compo-
236 sitions, origins, and modulation of CRs (GCRs and ACRs) and SEPs. However, in order
237 to deepen our understanding of CRs and SEPs' characteristics, we would combine the
238 data analysis and the CR modulation models [e.g., *Zhao et al.*, 2013] and SEP transport
239 models [e.g., *Qin et al.*, 2006] to numerically study the variations of CRs and SEPs over
240 solar cycles.

241 **Acknowledgments.** We are partly supported by grants NNSFC 41374177, NNSFC
242 41125016. The data sets of SIS and CRIS are downloaded from the ACE Science Center
243 archives at <http://www.srl.caltech.edu/ACE/ASC/level2/>. We also acknowledge the use
244 of the sunspot number data provided to the community by NASA.

References

- 245 George, J. S., et al., Elemental composition and energy spectra of galactic cosmic rays
246 during solar cycle 23, *Astrophys. J.*, 698(2), 1666, 2009.
- 247 Goring, D. G., and V. I. Nikora, Despiking acoustic doppler velocimeter data, *Journal of*
248 *Hydraulic Engineering*, 128(1), 117–126, 2002.
- 249 Laurenza, M., G. Consolini, M. Storini, and A. Damiani, A Shannon entropy approach to
250 the temporal evolution of SEP energy spectrum, *Astrophys. Space Sci. Trans.*, 8, 19–24,
251 doi:10.5194/astra-8-19-2012, 2012.
- 252 Qin, G., M. Zhang, and J.-R. Dwyer, The effect of adiabatic cooling on the fitted par-
253 allel mean free path of solar energetic particles, *J. Geophys. Res.*, 111, A08,101, doi:

254 10.1029/2005JA011512, 2006.

255 Qin, G., L.-L. Zhao, and H.-C. Chen, Despiking of Spacecraft Energetic Proton Flux
256 to Study Galactic Cosmic-Ray Modulation, *Astrophys. J.*, *752*, 138, doi:10.1088/0004-
257 637X/752/2/138, 2012.

258 Reames, D.-V., Element Abundances in Solar Energetic Particles and the Solar Corona,
259 2013.

260 Stone, E. C., A. M. Frandsen, R. A. Mewaldt, E. R. Christian, D. Margolies, J. F. Ormes,
261 and F. Snow, The Advanced Composition Explorer, *Space Sci. Rev.*, *86*, 1–22, doi:
262 10.1023/A:1005082526237, 1998.

263 Zhao, L.-L., and G. Qin, An observation-based GCR model of heavy nuclei: Measure-
264 ments from CRIS onboard ACE spacecraft, *J. Geophys. Res.*, *118*(5), 1837–1848, doi:
265 10.1002/jgra.50235, 2013.

266 Zhao, L.-L., G. Qin, M. Zhang, and B. Heber, Modulation of galactic cosmic rays during
267 the unusual solar minimum between cycles 23 and 24, *J. Geophys. Res.*, submitted,
268 2013.

Table 1. Recommended energy in unit of MeV/nuc of each measurement energy intervals of ACE/SIS obtained from ACE Home page (<http://www.srl.caltech.edu/ACE/ASC/>).

Element	E_1	E_2	E_3	E_4	E_5	E_6	E_7	E_8
<i>He</i> (2)	4.0	5.4	6.7	8.4	11.5	15.6	23.0	34.8
<i>C</i> (6)	7.4	9.8	12.3	15.5	21.2	28.9	42.5	64.4
<i>N</i> (7)	8.0	10.7	13.3	16.9	23.1	31.4	46.3	70.2
<i>O</i> (8)	8.5	11.4	14.3	18.1	24.8	33.8	49.8	75.7
<i>Ne</i> (10)	9.5	12.8	16.0	20.4	28.0	38.2	56.4	85.8
<i>Na</i> (11)	9.6	13.0	16.4	20.8	28.7	39.3	58.0	88.2
<i>Mg</i> (12)	10.3	14.0	17.6	22.4	30.9	42.2	62.4	95.0
<i>Al</i> (13)	10.4	14.1	17.8	22.8	31.5	43.1	63.8	97.3
<i>Si</i> (14)	11.0	15.0	18.9	24.2	33.4	45.8	67.9	103.6
<i>S</i> (16)	11.6	15.9	20.2	25.8	35.8	49.2	73.0	111.7
<i>Ar</i> (18)	12.1	16.9	21.5	27.7	38.5	53.2	79.1	121.2
<i>Ca</i> (20)	12.6	17.5	22.4	28.8	40.1	55.3	82.4	126.6
<i>Fe</i> (26)	13.0	18.5	23.8	30.9	43.5	60.6	90.9	140.4
<i>Ni</i> (28)	13.7	19.5	25.2	32.7	46.2	64.4	96.7	149.7

Table 2. Energy channels shown in Table 1 for elements N, O, and Fe.

Channel	$E_i(\text{MeV/nuc})$	E_i		
		Fe	Ni	O
I	13	E_1	E_1	E_3
II	31	E_4	E_4	E_6
III	46	E_5	E_5	E_7

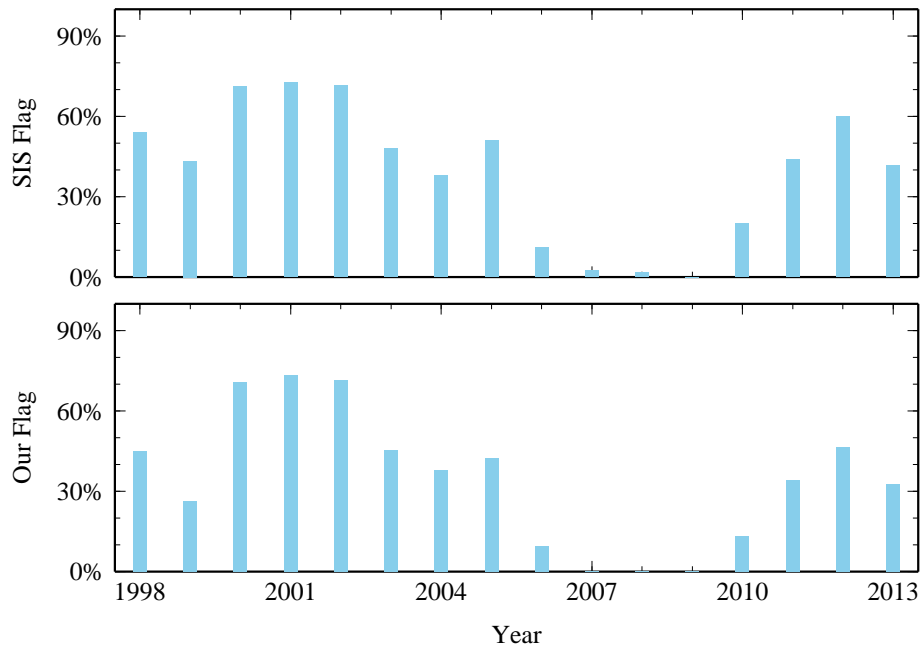


Figure 1. The percentage of flagged periods in each year with SIS flag (top panel) and our flag (bottom panel).

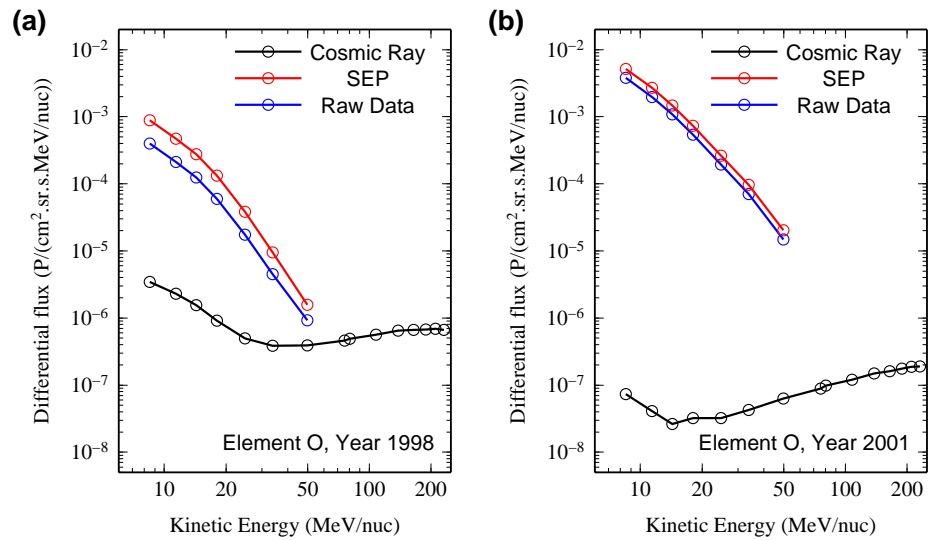


Figure 2. The kinetic energy spectra of element O for year 1998 (left panel) and year 2001 (right panel). The blue, red, and black lines indicate raw data from SIS measurements, SEP data from flagged periods, and CR background data from the non-flagged periods, respectively.

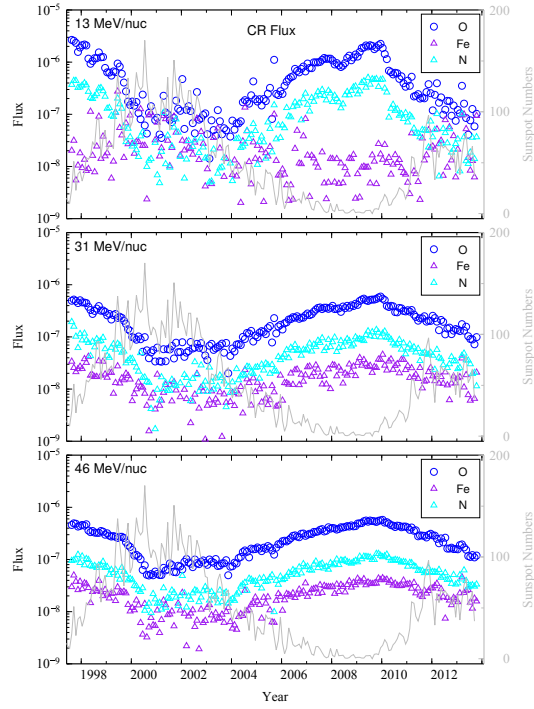


Figure 3. CR fluxes of O (blue circles), Fe (purple triangles), and N (cyan triangles), corresponding to the energy channels 13 MeV/nuc (top panel), 31 MeV/n (middle panel), and 46 MeV/nuc (bottom panel). Note that the grey line represents the time variations of sunspot number.

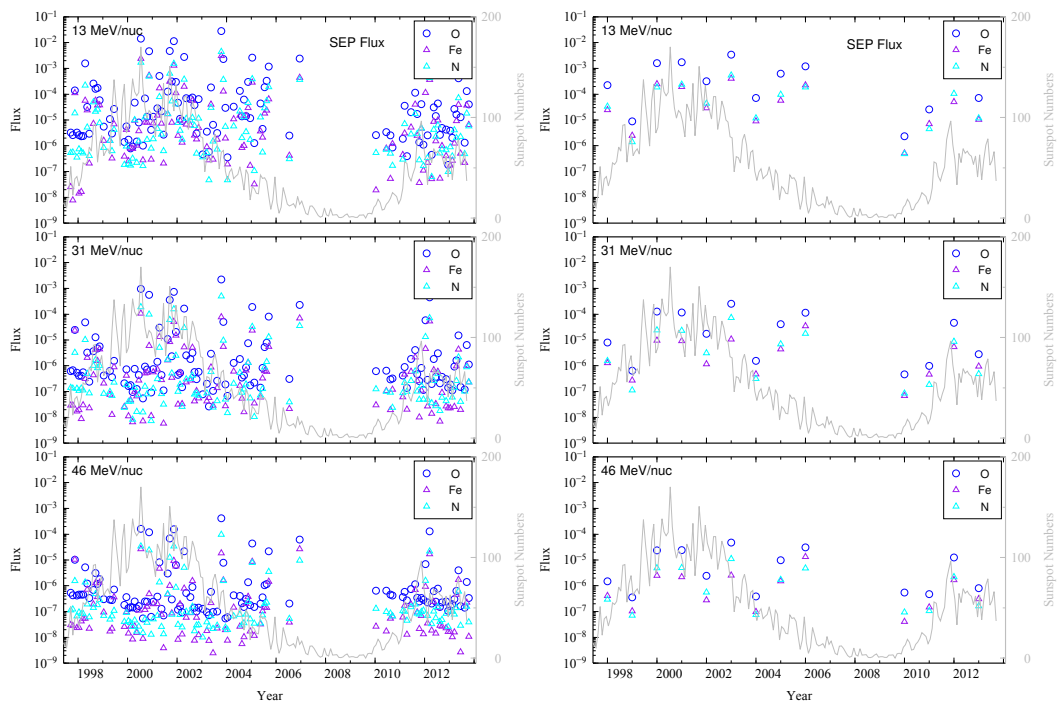


Figure 4. Similar as Figure 3 except that color symbols indicate SEP fluxes in monthly and yearly average in left and right panels, respectively.

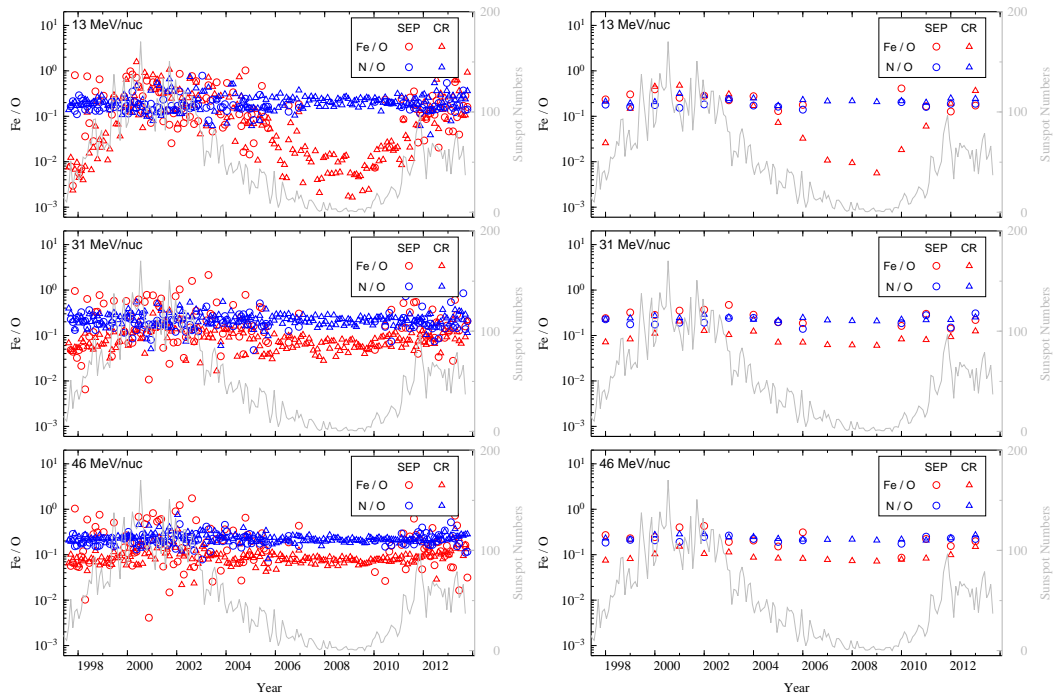


Figure 5. Similar as Figure 4 except that red and blue symbols indicate Fe/O ratio and N/O ratio, respectively, and that circles and triangles indicate SEPs and CRs, respectively.

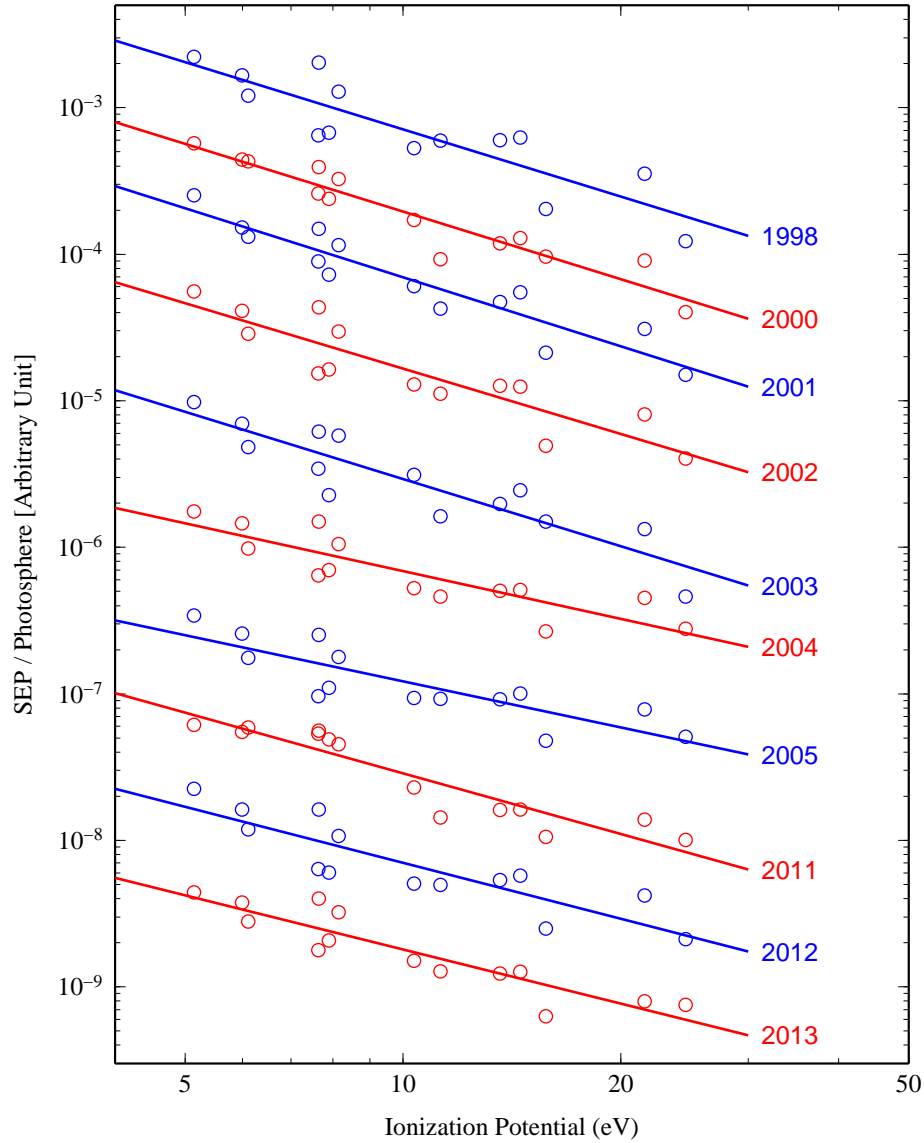


Figure 6. Fitted 15 MeV/nuc element fluxes for yearly average of SEP events relative to the recent photospheric abundances are shown as a function of FIP. The results are multiplied by a free number for presentation purpose. The solid lines are least-square linear fit in log-log space.

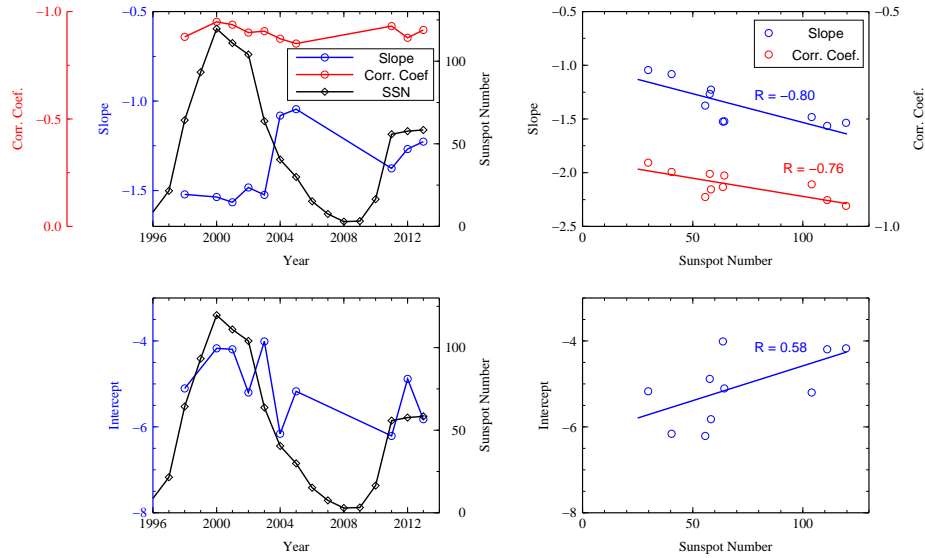


Figure 7. The slope, intercept, and correlation coefficients (Corr. Coef.) of the least-square linear fit in Figure 6 are shown. Top left panel shows the slope, Corr. Coef., and sunspot numbers (SSN) varying as the year. Top right panel shows the slope and Corr. Coef. varying as the SSN, and linear-fit of the slope and Corr. Coef. as functions of SSN are also shown. Bottom left panel shows the intercept and SSN varying as the year. Bottom right panel shows the intercept as a function of the SSN, and the linear-fit is also shown.

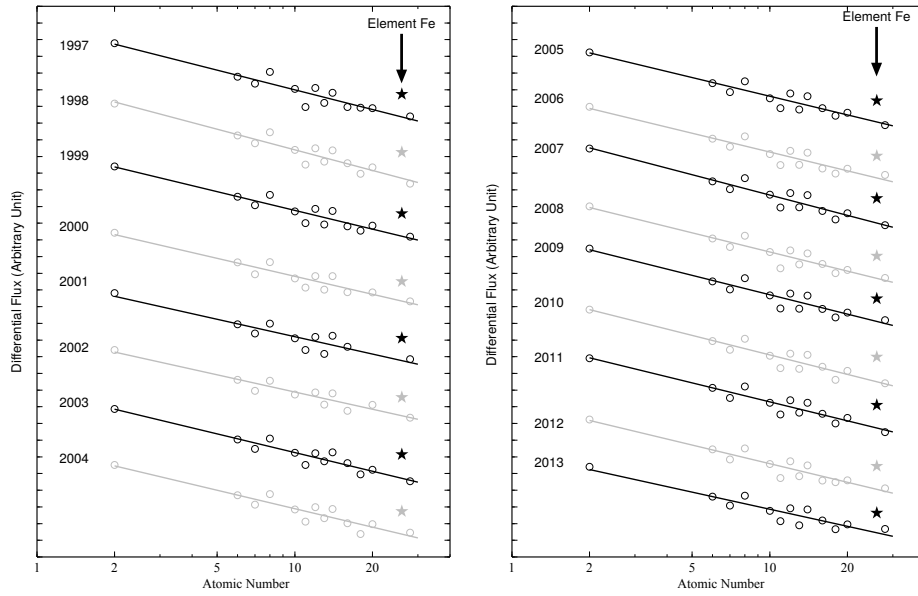


Figure 8. Fitted 30 MeV/nuc element fluxes for yearly average of GCRs are shown as a function of atomic numbers. The results are multiplied by a free number for presentation purpose. The solid lines are the least-square linear fit in log-log space. The solid star indicates the element Fe and are not included in the linear fit.

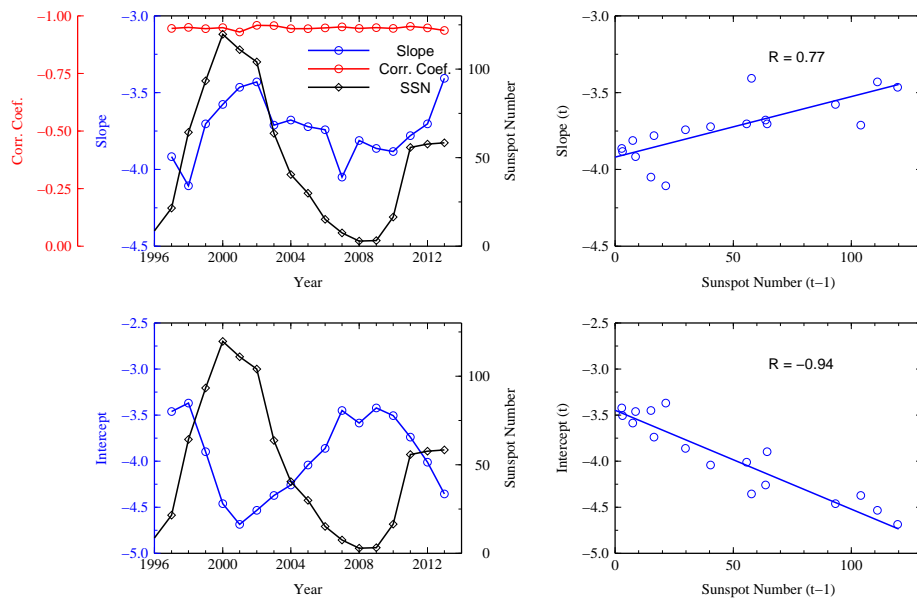


Figure 9. Similar as in Figure 7, the fitting results in Figure 8 are shown, except in top right panel the Corr. Coef. are not shown.

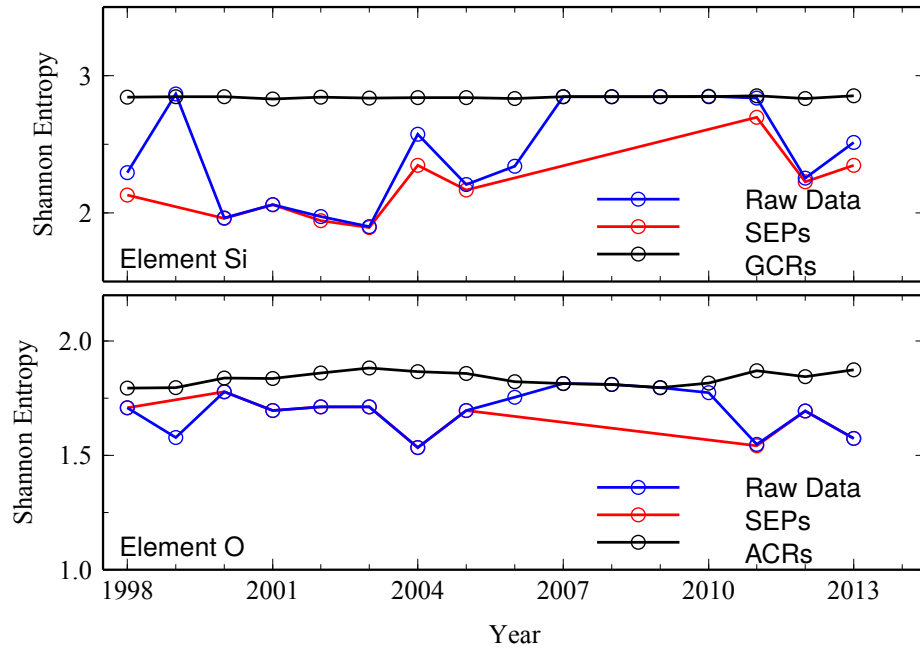


Figure 10. The entropy of element Si with all ACE/SIS energy channels (11.0 MeV/nuc - 103.6 MeV/nuc) and that of element O with the first four ACE/SIS energy channels (< 20 MeV/nuc) over the period from the year 1998 to 2013. The entropy of raw data, SEPs and CRs are denoted as blue, red and black lines, respectively. The entropy of SEPs in the years 1999, and 2006-2010 are not included.